CHEMISTRY
A EUROPEAN JOURNAL

DOI: 10.1002/chem.200500623

Self-Assembled, Kinetically Locked, Ru^{II}-Based Metallomacrocycles: Physical, Structural, and Modeling Studies

Paul de Wolf,[b] Phil Waywell,[b] Matt Hanson,[b] Sarah L. Heath,*[a] Anthony J. H. M. Meijer,*[b] Simon J. Teat,[c] and Jim A. Thomas*[b]

Abstract: By using a "complex as ligand approach," the metal-ion-templated self-assembly of heterometallic teteranuclear metallomacrocycles containing kinetically locked Ru^{II} centers is described. Depending on the metal-ion template employed in the self-assembly process, the final macrocycle can be kinetically labile or inert. Electrochemical studies reveal that the kinetically inert macrocycles display reversible $Ru^{III/II}$ oxidation couples. The crystal structure of a kinetically inert Ru_2Re_2 macrocycles reveals a structurally complex palmate anion-binding pocket. Host–guest studies carried out with the same macrocycle in organic solvents reveals that the complex functions as a luminescent sensor for anions and that binding affinity and luminescent modulation is dependent on the structural nature and charge of the guest anion. Computational density functional theory (DFT) studies support the hypothesis that the luminescence of the macrocycle is from a ^{3}MLCT state and further suggests that the observed guest-induced luminescence changes are most likely due to modulation of nonradiative decay processes.

Keywords: density functional calculations · molecular recognition · ruthenium · self-assembly · sensors

Introduction

Currently there is a great deal of interest in the metal-coordination-templated construction of 2D and 3D architectures.[1] Much of this work has centered on kinetically labile, square-planar metal geometries,[2] (e.g., Pd^{II}). The advantage of using such moieties is that the self-assembly process is under thermodynamic control. Therefore, unlike conventional covalent chemistry—which typically yields kinetic product—entropy–enthalpy compensation effects predominate, thus yielding discrete, often highly complex architectures. The disadvantage of using such an approach is that the final product is, by definition, an equilibrium product and, as such, is not kinetically robust. Therefore, changes to equilibrium conditions may result in disassembly of the previously thermodynamic product.[3] This can be problematical as, in many cases, the construction of molecular devices for hosts, sensors, and molecular electronics will require kinetically robust architectures. Fujita and colleagues have shown that Pt^{II} centers, which in normal ambient conditions are kinetically inert, become relatively labile at elevated temperatures and in highly polar media or in the presence of a suitable template. Using this effect, they have isolated macrocyclic, catenated, and nanosized cage architectures. Unlike their Pd^{II}-based analogues these structures are remarkably stable. For example, the isolated catananes do not dissociate at temperatures as high as 100 °C; furthermore, addition of excess $[Pt(en)(NO_3)_2]$ (en = ethylene diimine) to the square macrocycle constructed in this manner does not lead to any sign of subsequent product redistribution.[4] However, this approach has yet to be systematically applied to metals that form octahedral complexes. The inclusion of such metal centers in kinetically locked architectures is appealing as, apart from supplying a structurally more complex connecting motif, octahedral centers can also possess attractive photo-

[a] Dr. S. L. Heath
Department of Chemistry
University of Manchester
Oxford Road, Manchester, M13 9PL (UK)
Fax: (+44) 161-275-4598
E-mail: sarah.l.heath@man.ac.uk

[b] Dr. P. de Wolf, P. Waywell, M. Hanson, Dr. A. J. H. M. Meijer, Dr. J. A. Thomas
Department of Chemistry
University of Sheffield
Sheffield S3 7HF (UK)
Fax: (+44) 114-222-9346
E-mail: a.meijer@sheffield.ac.uk
james.thomas@sheffield.ac.uk

[c] Dr. S. J. Teat
Daresbury Laboratory
Daresbury, Warrington, Cheshire WA4 4AD (UK)

physical, electrochemical, and catalytic properties that can be exploited in the design of molecular devices. For example, the Hupp group and others have used octahedral d^6 Re^I metal centers to construct photophysically active host structures that have a variety of possible device applications, including luminescent sensing of anions.[5] However, despite their rich optical and electrochemical properties, other d^6 metals centers are much less reported, with examples of Ru^{II}-based systems, in particular, being scarce. Lees et al. have described the synthesis of large heterometallomacrocycles that incorporate polypyridyl Ru^{II} and Os^{II} fragments.[6] Although these structures are not hosts, they possess interesting energy-transfer properties. Similarly, Long and colleagues have reported the synthesis of $[Ru_4(cyclen)_4(pz)_4]^{9+}$ (cyclen = 1,4,7,10-tetraazacyclododecane, pz = pyrazine), a metallomacrocyclic square analogue of the well-studied Creutz–Taube ion.[7]

We have investigated systematic methods for the targeted construction of architectures incorporating kinetically locked Ru^{II} building blocks. In one such approach, we use [Ru([*n*]-ane-S_x)] centers to both add functionality *and* act as the "assembler" (that is, the template during the assembly process). We recently reported on the electron-transfer properties of a triangular, kinetically robust, $Ru^{III/II}$ mixed-valence bowl produced by this methodology.[8]

In another approach to such architectures, we have used kinetically locked mononuclear Ru^{II} complexes containing suitable ligands such as 2,2′:4,4″:4′,4‴-quarterpyridyl (qtpy) as building blocks in a "complex as ligand" methodology[9] to yield heterometallomacrocycles[10] such as $\mathbf{1}^{8+}$ and $\mathbf{2}^{4+}$. Here the assembler is another metal center with an established templating function.

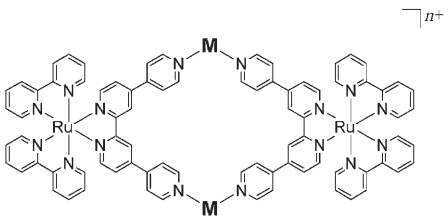

1, **M** = $[Pd(en)]^{2+}$; $n = 8$
2, **M** = $[ReCl(CO)_3]^{+}$; $n = 4$
3, **M** = $[Pt(en)]^{2+}$; $n = 8$

The ligand qtpy[11] was chosen as a suitable moiety for these studies as it allowed the construction of architectures containing previously reported $[Ru(bpy)_2(qtpy)]^{2+}$[12] fragments, which are related to the well-studied luminescent $[Ru(bpy)_3]^{2+}$ ion. Additionally, unlike simpler metallomacrocycles based on 4,4′-bpy,[1–7] the bi- and monodentate coordination modes of qtpy means that structures such as $\mathbf{1}^{8+}$ have two different "corner" angles. This was expected to create a structurally more complex central cavity. Previous work has revealed that due to efficient energy-transfer processes, luminescent emission of $\mathbf{1}^{8+}$ and $\mathbf{2}^{4+}$ is exclusively from the Ru^{II} ^{3}MLCT.[10] We now report further on the properties of **1** and **2**, and a newly synthesized Pt^{II} analogue (**3**), self-assembled by using $[Pt(en)Cl_2]$[13] as the assembler. The X-ray structural data obtained on **2** has also allowed us to carry out density function theory (DFT) calculations on the energetics of this system.

Results and Discussion

Complex $[\mathbf{3}](PF_6)_8$ was obtained through the reaction of $[Ru(bpy)_2(qtpy)]^{2+}$ with $[Pt(en)(NO_3)_2]$ in the same high-salt concentration conditions employed by Fujita and colleagues in the construction of homometallic Pt^{II} complexes.[4] This led to the isolation of the complex in moderate yield with no need for any elaborate workup. As might be expected from previous studies, complex **3** is more kinetically robust than its Pd^{II} analogue. Evidence of this effect can be seen in a comparison of 2D COSY spectra of the two complexes.

The spectrum of $[\mathbf{1}](PF_6)_8$ in $[D_3]$MeCN shows only signals associated with the complex and no impurities (Figure 1). It can be seen that the signals at $\delta = 8.52$ (B3, B3′), 8.07 (B4, B4′), 7.72 (B6, B6′), 7.43 (B5), and 7.36 ppm (B5′) correspond to bipy protons. The signals are more complex than expected due to the inequivalence of the two bipy rings. The signals at $\delta = 8.80$ (Q3), 7.89 (Q6), and 7.72 ppm (Q5) correspond to the protons on the inner qpy rings, whilst those at $\delta = 9.02$ (Q2′, Q6′) and 8.03 ppm (Q3′, Q5′) correspond to protons on the pendant pyridyl rings of qpy. A peak at $\delta = 2.85$ ppm, corresponding to the CH_2 units of the en ligand, is also observed. Although the NMR spec-

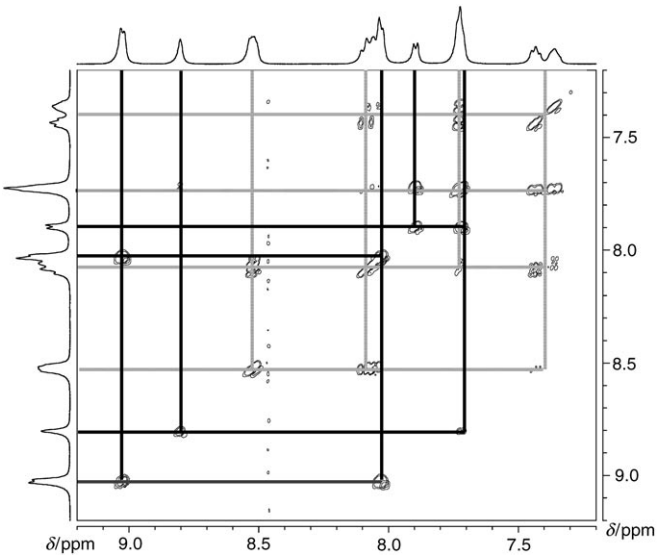

Figure 1. Aromatic region of the ^{1}H-COSY spectrum for $[\mathbf{1}](PF_6)_8$ in $[D_3]CH_3CN$ showing cross-coupling between bpy (light) and qtpy (bold) ligands.

trum of the isolated complex in $[D_3]$MeCN did not change, even after periods of days at room temperature, it was noticed that the spectrum of $[\mathbf{1}](PF_6)_8$ contained relatively broad signals and very little fine structure. This is due to the kinetic lability of the Pd^{II} metal center, with Pd–N bonds forming and breaking rapidly within the NMR timescale.

In contrast, the equivalent spectrum for the more kinetically robust $[\mathbf{3}](PF_6)_8$ shows much sharper, more well-defined signals (Figure 2). However, details of assignments are

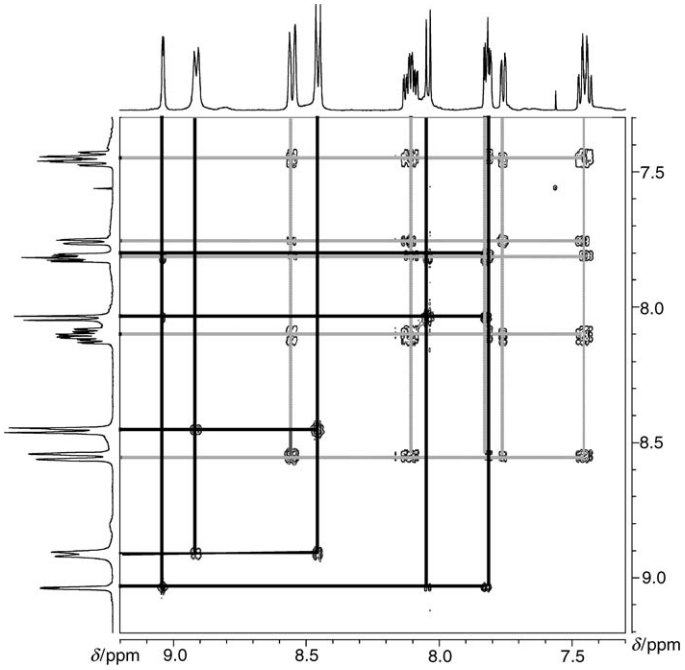

Figure 2. Aromatic region of the ^{1}H-COSY spectrum for $[\mathbf{3}](PF_6)_8$ in $[D_3]CH_3CN$ showing cross-coupling between bpy (light) and qtpy (bold) ligands.

very similar to that of **1**: the signals at $\delta = 8.55$ (B3, B3′), 8.10 (B4, B4′), 7.82 (B6), 7.76 (B6′), and 7.44 ppm (B5, B5′) correspond to bipy protons, while peaks at $\delta = 9.04$ (Q3), 8.04 (Q6), and 7.81 ppm (Q5) are assigned to the protons on the inner qpy rings. Signals at $\delta = 8.91$ (Q2′, Q6′) and 8.45 ppm (Q3′, Q5′) correspond to those on the pendant pyridyl rings and again an up-field signal, in this case at $\delta =$ 2.92 ppm, is assigned to the CH_2 units of the en ligand.

Electrochemical studies: There have been comparatively few studies on electroactive metallomacrocycles, particularly those containing Ru^{II} centers.[6,7] This is reflected by their scarcity in the literature. The electrochemical properties of the hexafluorophosphate salts of **1**, **2**, and **3** in acetonitrile were studied using cyclic voltammetry (Table 1).

Characteristic ligand-centered reductions were observed for each of the macrocycles. In all three complexes, the first and second observed waves are chemically reversible or quasi-reversible. Additionally, complexes $[\mathbf{1}](PF_6)_8$ and $[\mathbf{2}](PF_6)_4$ display a third reduction within the MeCN voltage

Table 1. Electrochemical data for the metallomacrocyclic complexes.[a]

	Oxidation $E_{1/2}$ [V] (ΔE_p [mV])	Reduction $E_{1/2}$ [V] (ΔE_p [mV])
1	+1.47[b]	−0.96(60), −1.27 (70), −1.50 (130)
2	+1.50 (90)	−0.99, (80) −1.25 (130)
3	+1.53 (80), +1.65 (80)	−0.85 (100), −1.07 (130), −1.41[b]

[a] Carried out at a scan rate of $100\,mV\,s^{-1}$ in acetonitrile containing 0.1 M TBAP as supporting electrolyte. Potentials were measured vs Ag/AgCl. E_{pa} quoted, associated stripping peak at $E_{pc} = 1.40$ V. [b] Peak not fully chemically reversible, therefore E_p is given.

window, which is chemically irreversible for $[\mathbf{2}](PF_6)_4$. No comparable reduction is observed for $[\mathbf{3}](PF_6)_8$. While all three macrocycles display oxidations at approximately 1.5 V, which are consistent with $Ru^{III/II}$-based couples, closer analysis of these processes reveal considerable differences (Table 1, Figure 3).

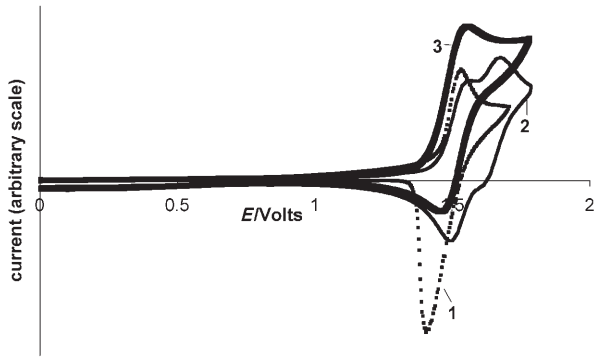

Figure 3. Cyclic voltammetry data for the oxidation of $[\mathbf{1}](PF_6)_8$, $[\mathbf{2}](PF_6)_4$, and $[\mathbf{3}](PF_6)_8$.

The simplest behavior is exhibited by $[\mathbf{3}](PF_6)_8$, which displays a single reversible oxidation couple ($\Delta E < 100$ mV, $|I_a/I_c| = 1$) centered at 1.50 V (vs Ag/Agcl); this signal is anodically shifted by > 200 mV with respect to the $Ru^{III/II}$ couple for $[Ru(bpy)_2(qtpy)](PF_6)_2$.[12] As might be expected for two remotely connected metal centers, this result indicates that both of the Ru^{II} centers of $\mathbf{3}^{8+}$ are oxidized at the same potential.

By contrast, although $[\mathbf{1}](PF_6)_8$ displays an analogous cathodic wave at $E_{pa} = 1.54$ V, the return sweep reveals a stripping peak at 1.40 V. This indicates that on oxidation to $\mathbf{1}^{10+}$ the macrocyle decomposes, presumably resulting in a Ru^{III} species that is adsorbed onto the working electrode. It seems likely that the conversion of electron-donating Ru^{II} centers into electron-withdrawing Ru^{III} centers means that the monodentate pyridyl donor sites of the coordinated qtpy ligand become poorer donors for the kinetically labile Pd^{II} centers, thus leading to the disassembly of the macrocycle—a process that cannot occur in kinetically locked macrocycles **2** and **3**.

The oxidation of $\mathbf{2}^{4+}$ is different to that of $\mathbf{3}^{8+}$, as in this case, two close-lying reversible couples at 1.53 and 1.65 V are observed (Figure 3). The potential of the first couple is consistent with the simultaneous oxidation of Ru^{II} centers,

also observed for the other two macrocycles. However, unlike **1** and **3**, [**2**]$(PF_6)_4$ incorporates two different redox-active metal centers. Hence, we assign the second process observed for this complex to the simultaneous oxidation of the two Re^{I} centers. It is tempting to conclude that the separation between the Ru- and Re-based couples is due to an interaction between the adjacent redox-active metal centers. However, comparisons of mononuclear complexes involving the same ligand reveal that $Re^{II/I}$ couples usually occur at potentials that are more anodic, often by several hundred millivolts, than their $Ru^{III/II}$ analogues.[14] Thus, in reality, the two different metal centers are probably not interacting electrochemically to any large extent.

Structural studies: Very few structural studies on mixed-metal metallomacrocycles have been reported. To obtain further structural information on intermetallic distances and possible guest cavity sizes, we attempted to grow crystals of the metallomacrocycles using various counterions and solvent systems. We obtained crystals of [**2**]$(PF_6)_4$ by means of vapor diffusion of diethyl ether into a solution of the sample in nitromethane. Attempts to obtain crystals of the other macrocycles by using similar methods were unsuccessful. Although the crystals of [**2**]$(PF_6)_4$ were extremely weakly diffracting, it was possible to collect acceptable diffraction data by using a synchrotron radiation source (Table 2, Figure 4).

Table 2. Summary of crystallographic data for [**2**]$(PF_6)_4$.

formula	$C_{86}H_{60}Cl_2F_{24}N_{16}O_6P_4Re_2Ru_2$	a [Å]	22.499(2)
M_r	2638.82	b [Å]	22.733(2)
crystal system	triclinic	c [Å]	25.470(2)
space group	$P\bar{1}$	α [°]	111.001(2)
crystal size [mm]	$0.06\times0.06\times0.02$	β [°]	90.186(2)
ρ [$Mg\,m^{-3}$]	1.457	γ [°]	97.788(2)
$R1$ [$I>2\sigma(I)$]	0.0691	V [$Å^3$]	12030.2(19)
$wR2$ [$I>2\sigma(I)$]	0.2066	Z	4
$R1$ (all data)	0.0939	$F(000)$	5136
$wR2$ (all data)	0.2194		

The structure shows that all metal centers possess octahedral geometries with the quaterpyridyl ligand binding in a bidentate fashion to the Ru^{II} metal centers and in a monodentate fashion to the Re^{I} metal centers. Details of bond lengths and angles are summarized in Table 3.

It should be pointed out that, while the Ru^{II} centers are chiral and can be found as Λ or Δ helices and the Re–Cl units can theoretically take up *syn* or *anti* configurations, only the configuration seen in Figure 4 is observed in the crystal structure. This structure may be the thermodynamic result of solution self-assembly processes, or perhaps it preferentially crystalizes due to optimal packing forces.

A distance of 14.70 Å separates the two Ru^{II} centers, whilst the corresponding intermetallic distance between the two Re^{I} centers is slightly shorter at 13.10 Å. To accommodate the contrasting bite angles of the bidentate Ru^{II} coordination site and the Re^{I} coordination site, the macrocycle takes up "puckered" boatlike geometry, reminiscent of a

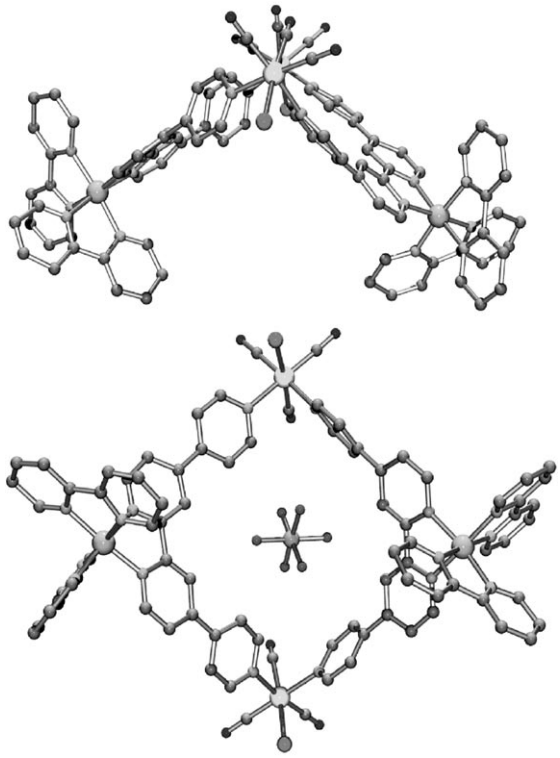

Figure 4. Crystal Structure of the cation of [**2**]$(PF_6)_4$. Hydrogen atoms removed for clarity. Top: View down Re–Re axis. Bottom: Orthogonal view showing hexafluorophosphate anion residing in central cavity.

cupped palm, with the axes occurring about the Re^{I} centers (Figure 4, top).

Interestingly, although three of the hexafluorophosphate ions are disordered between macrocyclic cations, the central cavity of the host is occupied by one of the PF_6^- counterions (Figure 4, bottom). This anion is precisely located in the center of the palm-like cavity, exactly bisecting the Re–Re plane.

Binding studies involving 2^{4+}—sensing anions: Previous work with water-soluble salts of **1** and **2** have revealed that they function as hosts for polyaromatic molecules.[10] However, in this case, the recognition process has no effect on the emission properties of the macrocycles.

The X-ray structure of [**2**]$(PF_6)_4$ reveals that this macrocycle also functions as a host for anions and that the binding pocket of this receptor is considerably more complex than that of previously reported 4,4′-bpy-based metallo-square complexes. Therefore the anion binding properties of **2** in acetonitrile were investigated.

The absorption spectrum of [**2**]$(PF_6)_4$ in acetonitrile is virtually identical to that of the previously reported [**2**]$(NO_3)_4$ in water and, as expected, photoexcitation at 480 nm leads to broad unstructured emission from the Ru–^{3}MLCT state centered at 665 nm. We then investigated the effect of anion concentration on this luminescence.

It was found that, although there was no shifting of emission wavelength, titration of NH_4BF_4 into a solution of [**2**]-

Table 3. Selected bond lengths [Å] and angles [°] for complex [**2**]$(PF_6)_4$.

Re(1)−C(81)	1.902(11)	Re(2)−C(84)	1.906(11)	Ru(1)−N(1)	2.062(8)	Ru(2)−N(9)	2.054(9)
Re(1)−C(82)	1.902(10)	Re(2)−C(85)	1.916(11)	Ru(1)−N(2)	2.046(9)	Ru(2)−N(10)	2.056(11)
Re(1)−C(83)	2.064(11)	Re(2)−C(86)	2.131(13)	Ru(1)−N(3)	2.065(9)	Ru(2)−N(11)	2.058(10)
Re(1)−N(7)	2.218(7)	Re(2)−N(8)	2.231(8)	Ru(1)−N(4)	2.077(7)	Ru(2)−N(12)	2.051(9)
Re(1)−N(16)	2.223(8)	Re(2)−N(15)	2.209(8)	Ru(1)−N(5)	2.029(7)	Ru(2)−N(13)	2.065(9)
Re(1)−Cl(1)	2.436(4)	Re(2)−Cl(2)	2.435(4)	Ru(1)−N(6)	2.055(7)	Ru(2)−N(14)	2.038(8)
C(82)-Re(1)-C(81)	89.8(5)	C(83)-Re(1)-N(16)	89.8(3)	C(84)-Re(2)-C(85)	88.2(5)	C(86)-Re(2)-N(8)	90.9(2)
C(82)-Re(1)-C(83)	89.7(5)	N(7)-Re(1)-N(16)	81.3(3)	C(84)-Re(2)-C(86)	92.3(5)	N(15)-Re(2)-N(8)	83.8(3)
C(81)-Re(1)-C(83)	88.1(5)	C(82)-Re(1)-Cl(1)	88.0(4)	C(85)-Re(2)-C(86)	87.4(4)	C(84)-Re(2)-Cl(2)	91.9(4)
C(82)-Re(1)-N(7)	177.7(4)	C(81)-Re(1)-Cl(1)	95.7(4)	C(84)-Re(2)-N(15)	177.0(3)	C(85)-Re(2)-Cl(2)	92.2(3)
C(81)-Re(1)-N(7)	92.3(3)	C(83)-Re(1)-Cl(1)	175.6(3)	C(85)-Re(2)-N(15)	94.1(3)	C(86)-Re(2)-Cl(2)	175.8(3)
C(83)-Re(1)-N(7)	91.4(2)	N(7)-Re(1)-Cl(1)	90.8(2)	C(86)-Re(2)-N(15)	89.8(3)	N(15)-Re(2)-Cl(2)	86.1(2)
C(82)-Re(1)-N(16)	96.6(3)	N(16)-Re(1)-Cl(1)	86.70(19)	C(84)-Re(2)-N(8)	94.0(3)	N(8)-Re(2)-Cl(2)	89.2(2)
C(81)-Re(1)-N(16)	173.2(3)			C(85)-Re(2)-N(8)	177.3(3)		
N(5)-Ru(1)-N(2)	95.1(3)	N(6)-Ru(1)-N(3)	94.7(3)	N(14)-Ru(2)-N(12)	97.4(3)	N(9)-Ru(2)-N(10)	80.0(5)
N(5)-Ru(1)-N(6)	78.8(3)	N(1)-Ru(1)-N(3)	96.9(3)	N(14)-Ru(2)-N(9)	176.0(4)	N(11)-Ru(2)-N(10)	175.0(4)
N(2)-Ru(1)-N(6)	90.3(3)	N(5)-Ru(1)-N(4)	95.3(3)	N(12)-Ru(2)-N(9)	86.1(3)	N(14)-Ru(2)-N(13)	78.8(3)
N(5)-Ru(1)-N(1)	173.2(3)	N(2)-Ru(1)-N(4)	98.4(4)	N(14)-Ru(2)-N(11)	85.8(4)	N(12)-Ru(2)-N(13)	174.9(3)
N(2)-Ru(1)-N(1)	78.7(4)	N(6)-Ru(1)-N(4)	169.9(3)	N(12)-Ru(2)-N(11)	80.6(4)	N(9)-Ru(2)-N(13)	97.8(3)
N(6)-Ru(1)-N(1)	98.2(3)	N(1)-Ru(1)-N(4)	88.5(3)	N(9)-Ru(2)-N(11)	96.7(4)	N(11)-Ru(2)-N(13)	95.6(3)
N(5)-Ru(1)-N(3)	89.5(3)	N(3)-Ru(1)-N(4)	76.9(3)	N(14)-Ru(2)-N(10)	97.6(4)	N(10)-Ru(2)-N(13)	88.6(4)
N(2)-Ru(1)-N(3)	173.7(3)			N(12)-Ru(2)-N(10)	95.3(4)		

$(PF_6)_4$ in acetonitrile led to a progressive enhancement in luminescence intensity of the host macrocycle (Figure 5). This enhancement was of a similar magnitude to that observed for a Re^I-based luminescent macrocycle reported by Hupp et al.[5a,b] This interaction is not due to simple, nonspecific electrostatic ion-pairing effects, as titrations involving the $[Ru(bpy)_2(qtpy)]^{2+}$ ion resulted in no detectable luminescent changes.

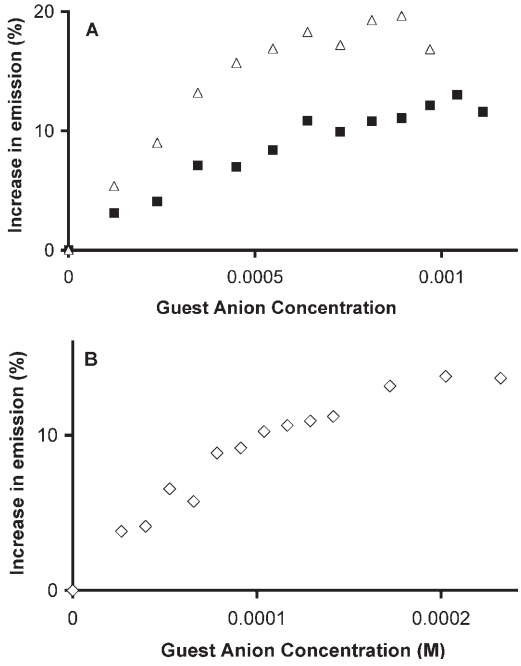

Figure 5. Representative luminescent titrations of anion guest with [**2**]$(PF_6)_4$. A) ■ = BF_4^-, △ = BPh_4^-; B) ◇ = SO_4^{2-}. Concentration of host = 5.75×10^{-5} M.

To further investigate this effect, the binding of a larger anion (BPh_4^-) and a dication (SO_4^{2-}) were investigated. These studies revealed that in both cases, and especially for BPh_4^-, addition of anion to solutions of [**2**]$(PF_6)_4$ in MeCN resulted in a more pronounced luminescent enhancement relative to that observed with to BF_4^- and that, particularly for SO_4^{2-}, the effect saturates at lower anion concentration (Figure 5).

Estimates of binding affinities were obtained through fits of the changes in luminescence to a 1:1 binding model (Table 4).

Table 4. Estimates of binding constants for selected anions with [**2**]$(PF_6)_4$.

Anionic guest	K_b [M^{-1}]	Anionic guest	K_b [M^{-1}]
BF_4^-	1575	BPh_4^-	2895
SO_4^{2-}	7135		

The binding affinity of **2** for SO_4^{2-} is higher than those reported for simple homometallic systems based on 4,4′-bpy,[5b] being almost five times that for BF_4^-. Since both these anions are of similar size and geometry, it is clear that electrostatics do play an important part in the host–guest interaction of **2**. However, a comparison of the data obtained for the two mono-anions reveals that BPh_4^- is bound with almost double the affinity for BF_4^-, indicating that factors other than electrostatics also contribute. Previous work has established that in water, $\mathbf{2}^{4+}$ is a host for polycyclic aromatic molecules. Therefore, we conclude that, even in acetonitrile, π–π interactions also play a significant part in the recognition of BPh_4^-.

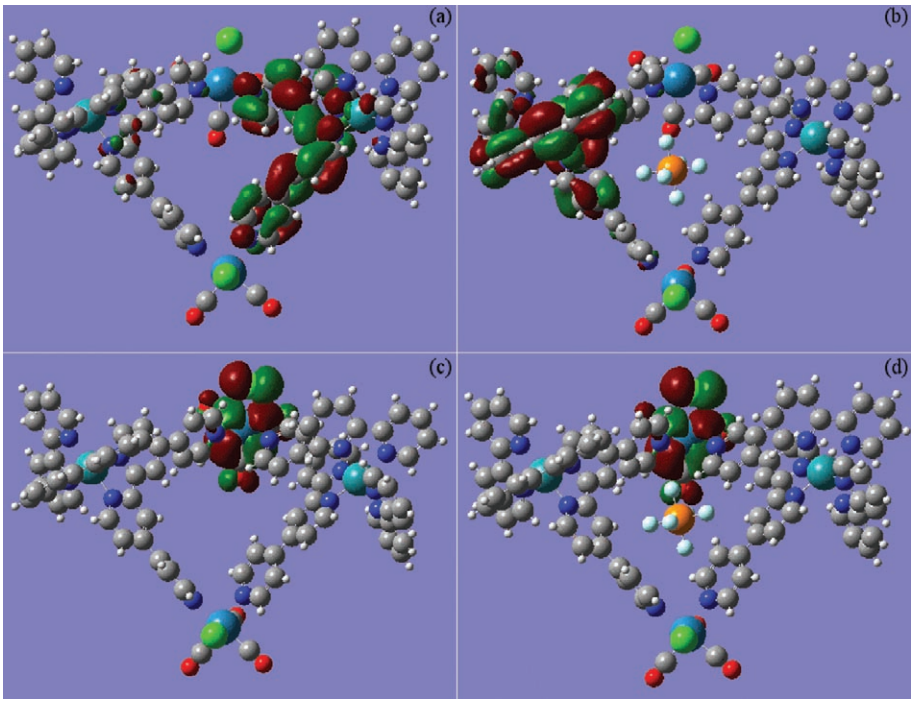

Figure 6. Pictorial representation of the HOMOs of a) the ^{3}MLCT state and c) the ^{1}A state of $[\mathbf{2}]^{4+}$ and the HOMOs of b) the ^{3}MLCT state and d) the ^{1}A state of $[\mathbf{2}{+}PF_6]^{3+}$.

Computational studies: The highest occupied molecular orbitals (HOMOs) of $[\mathbf{2}]^{4+}$ and $[\mathbf{2}{+}PF_6]^{3+}$ are plotted in Figure 6. This figure clearly shows that excitation can be characterized as metal-to-ligand charge transfer (MLCT), with the electron excited from the ground-state singlet state (^{1}A) to the first excited triplet state (^{3}MLCT). The calculations, indicating that the HOMO is a Re^{I}-based state while the triplet state involves the Ru^{II}-center, are consistent with previous experimental studies that have revealed that photoexcitation of any MLCT or π–π^* excited state results in relaxation to the lowest lying Ru–^{3}MLCT state. Although no contribution from PF_6^- is noticeable, the HOMOs of the ^{3}MLCT states in panels a and b in Figure 6 are slightly different. This effect is due to the fact that in $\mathbf{2}^{4+}$, the lowest unoccupied molecular orbitals (LUMOs) in the ^{1}A state lie very close together. As a result, a small disturbance in the electric field surrounding the molecule results in large mixing of the orbitals without a large change in electronic energy; however, the differences in the HOMOs (shown in Figure 6a and b) are not thought to be a significant.

This effect is also clear through an examination of the energy differences between the ^{1}A and ^{3}MLCT states (Table 5). These numbers were calculated by using the ΔSCF approach.[15] In this method, the energy difference between the ^{1}A and ^{3}MLCT states is obtained by optimizing the two states separately. The top line in Table 5 includes solvent effects, whereas in the bottom line the calculations are done in vacuo. The results show that the emission wavelength changes by only 0.00141096 au or 12 nm between $[\mathbf{2}]^{4+}$ and $[\mathbf{2}{+}PF_6]^{3+}$, thus confirming the experimental observation that the addition of PF_6^- has little or no effect on the measured emission wavelength. Although the overall emission wavelengths found are shorter than the 665 nm measured in the experiment, given the inaccuracies in the calculation—particularly the (partial) neglect of electron correlation and the use of pseudo potentials—the figures obtained show an excellent agreement between theory and experiment.

Even though the addition of PF_6^- has only a small effect on the emission wavelength, the experiments show an increase in the intensity of the steady-state emission upon addition of PF_6^-. Thus, it seems likely that PF_6^- changes the ratio between the rates of radiative and nonradiative decay of the ^{3}MLCT state. Enhancement of the rate of radiative decay upon addition of PF_6^- would be indicated by an increase in the oscillator strength for the transition. Unfortunately, it is not straight forward to calculate this quantity with the ΔSCF method, since the singlet and triplet wave functions are not orthogonal as they were optimized separately. This quantity would normally be calculable by means of the time-dependent DFT method, which would also give the singlet–triplet splitting. However, it fails for long-distance charge-transfer transitions, as in our case.[16] Nonetheless, the lack of change in the excitation wave length upon addition of PF_6^- suggests that the oscillator strength for the transition is unperturbed, indicating that the enhancement of the quantum yield is caused by a reduction in the rate of nonradiative decay. Hupp and co-workers suggested that a similar effect observed in kinetically labile Re/Pd, 4,4′-bpy-based systems is due to an electrostatic effect, whereby the bound anion affects Pd^{II}-based quenching of the Re–^{3}MLCT-centered emission.[5a] An alternative explanation is that the addition of an ion in the middle of the macrocycle stiffens the torsions of the pyridine rings, thereby making

Table 5. Transition energies and emission wavelengths for the ^{3}MLCT–^{1}A transition.

	$[\mathbf{2}]^{4+}$		$[\mathbf{2}{+}PF_6]^{3+}$	
	$\Delta E(^3\text{MLCT}-^1\text{A})$ [au]	$\lambda(^3\text{MLCT}-^1\text{A})$ [nm]	$\Delta E(^3\text{MLCT}-^1\text{A})$ [au]	$\lambda(^3\text{MLCT}-^1\text{A})$ [nm]
solvent	0.07620299	597.92	0.07479203	609.20
in vacuo	0.11077651	410.56	0.09587523	475.24

nonradiative transfer less favorable. The fact that the largest anion, BPh_4^-, induces the greatest enhancement in luminescence and not the anion that is bound with the highest affinity, SO_4^{2-}, suggests that this latter hypothesis is more likely. However, we are currently investigating the origin of the increase in the quantum yield in more detail.

The difference between the top and bottom lines of Table 5 also clearly shows that inclusion of the solvent in the calculations is imperative in obtaining reasonable agreement with experimental data. Moreover, the comparison of the two lines also shows that the influence of addition of PF_6^- is clearly mitigated by the effect of the solvent.

Conclusions

By using a "complex as ligands" approach it is possible to construct kinetically inert metallomacrocycles from mononuclear Ru^{II} complex building blocks. The inclusion of such complexes into macrocyclic host architectures results in systems with rich photophysical and electrochemical properties. It has been found that through recognition processes driven by a combination of electrostatic and π–π interactions, these macrocycles can function as prototypical luminescent anion sensors.

Our calculations offer confirmation of luminescence experimental results and have given us an insight into their origins. Work is ongoing to further elucidate the experimental findings, in particular the origin of the increased quantum yield upon addition of an ion into the macrocycle.

More detailed studies on the photophysics, electrochemistry and host–guest chemistry of all the reported Ru^{II}-based macrocycles are underway and will be reported in due course. We will also extend the outlined synthetic methods to construct other, more complex, architectures and devices.

Experimental Section

Materials: Commercially available materials were used as received. 2,2′:4,4″:4′,4″-Quarterpyridyl (qtpy),[11] $[Ru(bpy)_2(qtpy)](PF_6)_2$,[12] **[1]**$(PF_6)_8$, **[2]**$(PF_6)_4$,[10] and $[Pt(en)Cl_2]$[13] were all synthesized by means of adapted published procedures.

Instrumentation: ^{1}H NMR spectra were recorded on a Bruker AM250 machine working in Fourier transform mode. Mass spectral data was collected on a Micromass Prospec spectrometer operating in positive-ion fast-atom-bombardment (FAB^+) mode with a NOBA matrix. UV-visible spectra were recorded on Unicam UV2 or Varian-Carey bio-3 UV-visible spectrometers in twin-beam mode. Spectra were recorded in matched quartz cells (Helmer) and were baseline corrected. Emission spectra were recorded on a Hitachi F4500 spectrophotometer operating in luminescence wavelength scan mode. Elemental analyses were obtained using a Perkin–Elmer 2400 analyzer working at 975 °C.

Cyclic voltammograms were recorded by using an EG&G Versastat II potentiostat with the Electrochemistry Powersuite software package. A three-electrode cell was used with an Ag+/AgCl reference electrode separated from a Pt disk working electrode and Pt wire auxiliary electrode. Tetra-*n*-butylammonium hexafluorophosphate in acetonitrile (0.1 M dm^{-3}), doubly recrystalized from ethyl acetate/diethyl ether, was used as the support electrolyte.

Synthesis and characterization of [3](PF$_6$)$_8$: $[Pt(en)Cl_2]$ (0.165 g, 0.5 mmol) and $AgNO_3$ (0.17 g, 1 mmol) were stirred overnight in a 1:1 MeOH/H_2O solvent mixture (10 mL). The resulting AgCl that formed was removed by filtration through Celite. An aqueous solution of $[Ru(bpy)_2(qtpy)]Cl_2$ (0.40 g, 0.5 mmol) was added to the resulting $[Pt(en)(NO_3)_2]$ solution and enough KNO_3 was also added so that a 5 M KNO_3 solution was formed. This mixture was then heated at reflux for 24 h. A red/orange solid was precipitated by the addition of NH_4PF_6; the solid was collected by filtration and washed successively with H_2O (2×25 mL), EtOH (2×25 mL) and diethyl ether (4×20 mL). The solid was then redissolved in a minimum quantity of MeCN and re-precipitated with diethyl ether, collected by centrifuge, and dried in vacuo. Yield 0.61 g (39%); ^{1}H NMR ([D$_3$]MeCN): $\delta = 9.04$ (d, 4H), 8.91 (d, 8H), 8.55 (d, 8H), 8.45 (d, 8H), 8.10 (m, 8H), 8.04 (d, 4H), 7.82 and 7.75 (d, 8H) 7.81 (d, 4H), 7.45 (m, 8H), 4.35 (s, 8H), 2.92 ppm (s, 8H); elemental analysis calcd (%) for $Ru_2Pt_2C_{84}H_{76}N_{20}P_8F_{48}$: C 32.34, H 2.52, N 8.98; found: C 32.77, H 2.81, N 8.58.

Crystal structure determination: Crystals of **[2]**$(PF_6)_4$ were obtained by means of vapor diffusion of diethyl ether into a solution of the sample in nitromethane. Data were collected at 150(2) K on Station 9.8 at the Daresbury Laboratory on a Bruker SMART 1K CCD diffractometer equipped with an Oxford Cryostreams low-temperature attachment using silicon 111 monochromated synchrotron radiation ($\lambda = 0.6942$ Å). In all 77077 reflections were collected, 39962 were unique. All were used in the calculations. Although a number of crystals were tried, due to twinning, only one crystal gave a sensible unit cell. Even in this case, a careful examination of the diffraction pattern shows the presence of a second pattern at about 10% of the intensity of the main pattern —see cif file (available from CCDC; details given below) for full refinement details.

CCDC-234751 contains the supplementary crystallographic data for this paper. These data can be obtained free of charge from The Cambridge Crystallographic Data Centre via www.ccdc.cam.ac.uk/data_request/cif.

Computational methods: All calculations were performed by using the SMP version of the Gaussian 03 program package[17] with the B3LYP density functional method.[18] Gaussian 03 was compiled by using the Intel ifc compiler version 7.1 with ATLAS version 3.6.0[19] and the GOTO implementation of BLAS.[20]

The results turn out to be very sensitive to the basis sets employed. However, a rigorous discussion of basis set effects falls outside the scope of this paper and will be reported on elsewhere.[21] Thus, all calculations reported on here were performed by using Stuttgart/Dresden effective core potentials (SDD) on Ru and Re[22] and the 6–31G(d,p) basis set on all other atoms. As a result, the calculation contained 1992/2094 basis functions and 818/898 electrons for $[\mathbf{2}]^{4+}$ and $[\mathbf{2}{+}PF_6]^{3+}$, respectively. Overall symmetry was C_1. All calculations were performed with the crystal structure geometry and the assumption was made that the addition of PF_6^- to the macrocycle does not greatly affect its structure. Comparing the size of PF_6^- to the size of the cavity suggests that this was a reasonable approximation. We also performed geometry optimizations for $[\mathbf{2}]^{4+}$ and $[\mathbf{2}{+}PF_6]^{3+}$, but again they will be reported on elsewhere.[21] All calculations involving solvent were performed by using the Polarizable Continuum Model (PCM)[23] and the United Atom Topological Model[24] applied to radii optimized at the Hartree–Fock 6–31G(d) level of theory. This set of radii was used to retain compatibility with the implementation of PCM in earlier versions of Gaussian. The PCM equations were solved iteratively.

Acknowledgement

A.J.H.M.M. wishes to thank Prof. B. T. Pickup and Dr. M. J. Sykes for many stimulating discussions. S.L.H. and J.T. are grateful for financial support from the EPSRC (GR/M41193/01).

[1] a) S. Leininger, B. Olenyuk, P. J. Stang, *Chem. Rev.* **2000**, *100*, 853; b) G. F. Swiegers, T. J. Malefetse, *Chem. Rev.* **2000**, *100*, 3483; c) G. F. Swiegers, T. J. Malefetse, *Coord. Chem. Rev.* **2002**, *225*, 91.
[2] a) M. Fujita, *Chem. Soc. Rev.* **1998**, *27*, 214; b) M. Fujita, *Acc. Chem. Res.* **1999**, *32*, 53; c) M. Fujita, K. Umemoto, M. Yoshizawa, N. Fujita, T. Kusukawa, K. Biradha, *Chem. Commun.* **2001**, 509; d) P. J. Stang, *Acc. Chem. Res.* **2002**, *35*, 972.
[3] a) J. A. Thomas in *Encyclopedia of Supramolecular Chemistry* (Eds.: J. Steed, J. Atwood), Marcel Dekker, New York, **2004**; b) D. S. Lawrence T. Jiang, M. Levett, *Chem. Rev.* **1995**, *95*, 2229; c) D. B. Amabilino, J. F. Stoddart, *Chem. Rev.* **1995**, *95*, 2725.
[4] a) M. Fujita, F. Ibukuro, K. Yamaguchi, K. Ogura, *J. Am. Chem. Soc.* **1995**, *117*, 4175; b) F. Ibukuro, T. Kusukawa, M. Fujita, *J. Am. Chem. Soc.* **1998**, *120*, 8561.
[5] a) R. V. Slone, D. I. Yoon, R. M. Calhoun, J. T. Hupp, *J. Am. Chem. Soc.* **1995**, *117*, 11813; b) R. V. Slone, K. D. Benkstein, S. Bélanger, J. T. Hupp, I. A. Guzei, A. L. Rheingold, *Coord. Chem. Rev.* **1998**, *171*, 221; c) P. H. Dinolfo, J. T. Hupp, *Chem. Mater.* **2001**, *13*, 3113; d) M. H. Keefe, K. D. Benkstein, J. T. Hupp, *Coord. Chem. Rev.* **2002**, *225*, 91.
[6] a) S.-S. Sun, A. S. Silva, I. M. Brinn, A. J. Lees, *Inorg. Chem.* **2000**, *39*, 1344; b) S.-S. Sun, A. J. Lees, *Inorg. Chem.* **2001**, *40*, 3154.
[7] V. C. Lau, L. A. Berben, J. R. Long, *J. Am. Chem. Soc.* **2002**, *124*, 9042.
[8] N. Shan, S. Vickers, H. Adams, M. D. Ward, J. A. Thomas, *Angew. Chem.* **2004**, *116*, 4028; *Angew. Chem. Int. Ed.* **2004**, *43*, 3938.
[9] S. Serroni, S. Campagna, F. Puntoriero, C. Di Pietro, N. D. McClenaghan, F. Loiseau, *Chem. Soc. Rev.* **2001**, *30*, 367.
[10] P. de Wolf, S. L. Heath, J. A. Thomas, *Chem. Commun.* **2002**, 2540.
[11] R. J. Morgan, A. D. Baker, *J. Org. Chem.* **1990**, *55*, 1986.
[12] a) K. Bierig, R. J. Morgan, S. Tysoe, H. D. Gafney, T. C. Strekas, A. D. Baker, *Inorg. Chem.* **1991**, *30*, 4898; b) M. A. Hayes, C. A. Meckal, E. Schatz, M. D. Ward, *J. Chem. Soc. Dalton Trans.* **1992**, 703.
[13] G. W. Watt, D. H. Carter, *J. Inorg. Nucl. Chem.* **1969**, *31*, 1863.
[14] See, for example: a) D. A. Bardwell, F. Barigelletti, R. L. Cleary, L. Flamigni, M. Guardigli, J. C. Jeffery, M. D. Ward, *Inorg. Chem.* **1995**, *34*, 2438; b) C. Metcalfe, S. Spey, H. Adams, J. A. Thomas, *J. Chem. Soc. Dalton Trans.* **2002**, 4732; c) P. de Wolf, S. L. Heath, J. A. Thomas, *Inorg. Chim. Acta* **2003**, *355*, 280.
[15] a) T. Ziegler, A. Rauk, E. J. Baerends, *Theor. Chim. Acta* **1977**, *43*, 261; b) C. Daul, *Int. J. Quantum Chem.* **1994**, *52*, 867; See also c) T. Ziegler, J. Autschbach, *Chem. Rev.* **2005**, 105, 2695.
[16] See, for example: a) A. Dreeuw, J. Weisman, M. Head-Gordon, *J. Chem. Phys.* **2003**, *119*, 2943; b) D. Tozer, *J. Chem. Phys.* **2003**, *119*, 12697; c) D. J. Tozer, R. D. Amos, N. C. Handy, B. O. Roos, L. Serrano-Andrés, *Mol. Phys.* **1999**, *97*, 859, and references therein.
[17] Gaussian 03, Revision B.05, M. J. Frisch, G. W. Trucks, H. B. Schlegel, G. E. Scuseria, M. A. Robb, J. R. Cheeseman, J. A. Montgomery, Jr., T. Vreven, K. N. Kudin, J. C. Burant, J. M. Millam, S. S. Iyengar, J. Tomasi, V. Barone, B. Mennucci, M. Cossi, G. Scalmani, N. Rega, G. A. Petersson, H. Nakatsuji, M. Hada, M. Ehara, K. Toyota, R. Fukuda, J. Hasegawa, M. Ishida, T. Nakajima, Y. Honda, O. Kitao, H. Nakai, M. Klene, X. Li, J. E. Knox, H. P. Hratchian, J. B. Cross, V. Bakken, C. Adamo, J. Jaramillo, R. Gomperts, R. E. Stratmann, O. Yazyev, A. J. Austin, R. Cammi, C. Pomelli, J. W. Ochterski, P. Y. Ayala, K. Morokuma, G. A. Voth, P. Salvador, J. J. Dannenberg, V. G. Zakrzewski, S. Dapprich, A. D. Daniels, M. C. Strain, O. Farkas, D. K. Malick, A. D. Rabuck, K. Raghavachari, J. B. Foresman, J. V. Ortiz, Q. Cui, A. G. Baboul, S. Clifford, J. Cioslowski, B. B. Stefanov, G. Liu, A. Liashenko, P. Piskorz, I. Komaromi, R. L. Martin, D. J. Fox, T. Keith, M. A. Al-Laham, C. Y. Peng, A. Nanayakkara, M. Challacombe, P. M. W. Gill, B. Johnson, W. Chen, M. W. Wong, C. Gonzalez, J. A. Pople, Gaussian, Inc., Wallingford CT, **2004**.
[18] A. D. Becke, *J. Chem. Phys.* **1993**, *98*, 5648.
[19] R. C. Whaley, A. Petitet, J. J. Dongarra, *Parallel Comput.* **2001**, *27*, 3; also available as University of Tennessee LAPACK Working Note #147, UT-CS-00-448, **2000** (www.netlib.org/lapack/lawns/lawn147.ps).
[20] See http://www.cs.texas.edu/users/flame/goto.
[21] A. J. H. M. Meijer, J. A. Thomas, Ö. Farkas, work in progress.
[22] a) A. Nicklass, M. Dolg, H. Stoll, H. Preuss, *J. Chem. Phys.* **1995**, *102*, 8942; b) X. Y. Cao M. Dolg, *J. Chem. Phys.* **2001**, *115*, 7348, and references therein.
[23] a) B. Menucci, J. Tomassi, *J. Chem. Phys.* **1997**, *106*, 5151; b) M. Cossi, V. Barone, B. Menucci, J. Tomassi, *Chem. Phys. Lett.* **1998**, *286*, 253, and references therein.
[24] V. Barone, M. Cossi, J. Tomassi, *J. Chem. Phys.* **1997**, *107*, 3210.

Received: June 1, 2005
Published online: December 19, 2005

